ISSN: 2834-7706

Review Article

Journal of Mathematical Techniques and Computational Mathematics

Two Methods Used for Radiative Micropolar Nanofluid Passed Through a Porous Channel

Hossein Narimisa*

Besat Power Plant Tehran, Iran.

*Corresponding Author
Hossein Narimisa, Besat Power Plant Tehran, Iran.

Submitted: 2023, June 02; **Accepted:** 2023, June 20; **Published:** 2023, July 05

Citation: Narimisa, H. (2023). Two Methods Used for Radiative Micropolar Nanofluid Passed Through a Porous Channel. *J Math Techniques Comput Math, 2*(7), 308-316.

Abstract

In this study, radiative micropolar nanofluid passed through a porous channel was analyzed. Because of the considerable amount of difference, a Finite element technique with the approval of the AGM method was used. Different parameter and dimensionless numbers like Reynolds number Re, Hartman number M, the Thermophoretic number N_t with a variety of velocity, temperature, and concentration profile are shown graphically. There was no change in velocity or microrotation profile while there was a change in Reynolds number. Although the concentration profile decreased with increasing Reynolds number.

Keywords: MHD flow, Micropolar Nanofluid, AGM Method, Finite Element Technique, Radiation.

1. Introduction

Boundary layer flow of micropolar nanofluid towards a permeable stretching sheet in the presence of porous medium with thermal radiation and viscous dissipation was discussed by Kausar, Muhammad Salman, et al. By similarity solution they transfer their basic equations to ordinary equations and used the Runge–Kutta fourth–order to solve those equations [1].

Priya Mathur and Satyaranjan Mishra analyzed the Radiative Micropolar Nanofluid past through a Porous Channel with the use of an approximate analytical technique (ADM), the Adomian Decomposition Method, to solve ODEs which provided from similarity solution to change PDEs to ODEs [2].

Investigating a micropolar fluid flow in a channel that was subjected to a chemical reaction using the Differential Transformation Method (DTM) was done by M Sheikholeslami, HR Ashorynejad, DD Ganji. They have determined the effect of various parameters such as the Reynolds number, the coupling parameter, and the spin gradient viscosity parameter on the fluid properties [3].

Mohyud-Din, Syed Tauseef, et al. studied a flow of a radiative and electrically conducting micropolar nanofluid inside a porous channel. By performing the similarity solution, PDEs changed to ODEs. Equations solved via the HAM and Runge–Kutta methods [4].

Axisymmetric flow and heat transfer in an incompressible micropolar fluid between two porous discs have been studied by Takhar, Harmindar S., et al. who solved the system of nonlinear coupled differential equations by a finite element method. The results were shown graphically [5]. Analyzing the micro-polar nanofluid in a rotating system between two parallel plates with electric and magnetic fields has been done by Jalili, P., Narimisa, H., Jalili, B., Shateri, A., & Ganji, D. D. (2022). The governing equation is solved via numerical and semi-analytical methods [6].

Examination of a rotating system with a micro-polar nanofluid between two parallel plates in the presence of magnetic and electric fields has been done by Jalili, P., Narimisa, H., Jalili, B., & Ganji, D. D. (2023). The impacts of dimensionless parameters were discussed graphically [7]. Shah, Zahir, et al. investigated the MHD nanofluid flows between two rotating disks that have the same rotation speed, but in different directions. With the use of a similarity solution, they changed PDEs to ODEs, and the semi-analytical HAM method was used to solve the system of nonlinear equations [8].

2. Problem Description

According to fig 1 and previous work micropolar nanofluid passed through a porous channel [2-4]. Assuming $2h$ was the width of the channel so $y = +h$, was for the upper origin and vice versa $y = -h$. With a velocity equal to v_0 fluid is continuously injected or sucked. T_1, C_1 Are respectively derived as the temperature and T_2, C_2 solute concentration, and had the same role on the opposite side.

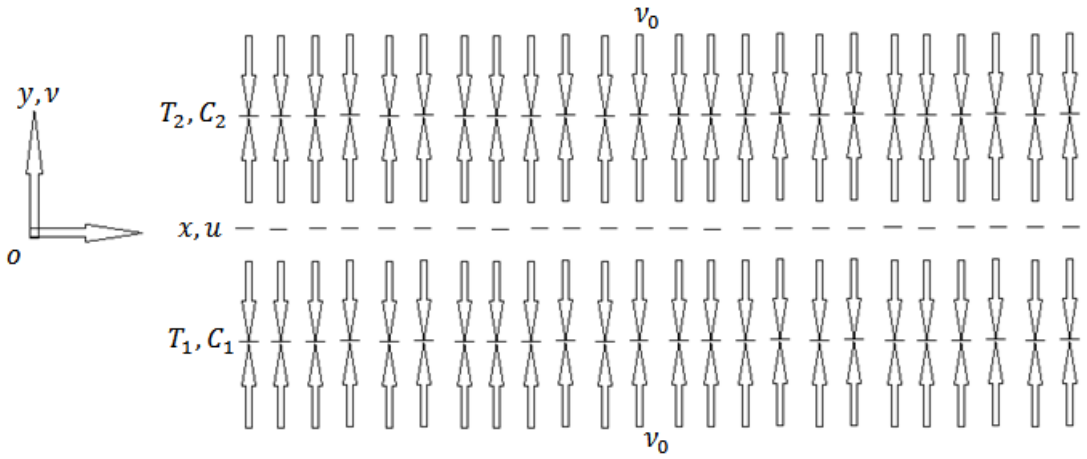

Figure 1: micropolar nanofluid passed through a porous channel

By skipping from the method, which derived the formulation (all have been spoken in previous works obtained formulation is listed as below [2-4]:

$$\begin{cases} (1+N_1)f^{iv} - R(ff''' - f'f'') - N_1 g''' - M^2 f'' = 0 \\ N_2 g'' + N_3 R(f'g - g'f) - N_1(2g - f'') = 0 \\ \left(1+\frac{4}{3}Rd\right)\theta'' + P_r R(f'\theta + f\theta') + P_r\, N_b\, \phi'\theta' + Pr\, Nt\, (\theta')^2 = 0 \\ \phi'' + ScRe(f'\phi - f\phi') + \frac{N_t}{N_b}\theta'' = 0 \end{cases} \tag{1}$$

And the boundary conditions are:

$$f(1) = 0\,, f'(1) = -1\,, f(-1) = 0\,, f'(-1) = 0\,, g(1) = 1\,, g(-1) = 0\,, \theta(1) = 0$$
$$\theta(-1) = 1\,, \phi(-1) = 0\,, N_b\phi'(1) + N_t\theta'(1) = 0 \tag{2}$$

From [2] with the help of [8] It's clear that:

$$N_1 = \frac{\hat{\kappa}}{\mu}\,, N_2 = \frac{\nu_s}{\mu h^2}\,, N_3 = \frac{j}{h^2}\,, Re = \frac{uL}{\nu}\,, M = BL\sqrt{\frac{\sigma}{\mu}}\,, R_d = {}^{4T_2^3}/_{kk^*}\,, Pr = \frac{\nu}{\alpha}\,,$$
$$Nb = \frac{\tau D_B C_h}{\alpha}\,, N_t = \left(\frac{D_T}{T_0}\right)\frac{T_2 - T_0}{\alpha}\,, Sc = \frac{\nu}{D}$$

N_1 is the coupling parameter while N_2 showing the spin gradient viscosity parameter, N_3 presents the micropolar fluid constant, *Re* demonstrates the Reynolds number, *M* displays the Hartman number, *Rd* is for the Radiation, *Pr* stands for the Prandtl number, N_b represents the Brownian motion parameter, *Nt* indicates the thermophoresis parameter, *Sc* detects the Schmidt number and *R* is probably the height of the channel.

As spoken before, physical quantities were obtained as fallow [4]:

$$Nu_x = \frac{q''_{y=} - hx}{k_1(T_1 - T_2)} = -\theta'(-1)$$
$$Sh_x = \frac{m''_{y=} - hx}{k_1(C_1 - C_2)} = 0 \tag{3}$$

3. Results and Discussion

This part illustrates the result of flowing radiative micropolar nanofluid passed through a porous channel. In this study, the Prandtl number is set to 6.2, which is one of the water properties. Fig. 2 shows that the velocity of the fluid decreased with enhancement of the Hatman number M. This could be due to the fact that variations in velocity near the walls of the channel are approximately zero. And from the inside, by increasing the Hatman number, the magnetic field will increase, and then it has a counter effect on the velocity of the flow. Fig 3 shows the enhancement in coupling parameters N_1 that causes the increase in velocity. Due to the formula, if N_1 is going to increase it means there is a diminishment in viscosity, so velocity will increase. According to the result of fig 4, there was no absolute change in velocity while the Reynolds number was increased. It may be as a result of different parameters having counter effects on each other and, nullifies, or in this case, the variation in velocity is independent of a change in the Reynolds number. Fig.5 indicated that there was a slight amount of accretion in velocity when parameter R was growth, but changes were very few and it seems that there is no change in velocity when the R parameter changes. In fig 6, with the increase in the Hartman number, the microrotation profile is raised. Interaction of nanoparticles enhances the heat and causes a reduction in dynamic viscosity so that velocity will rise. Fig 7 showed that with an increase in parameter N_1 microrotation profile decreased. According to the formula, this is because of an increase in the vertex viscosity. Fig 8 demonstrated that there was an enhancement in microrotation profile when spin gradient viscosity N_2 increased. Reduction in viscosity and increase in velocity causes the enhancement in velocity, N_2 so micro rotation will increase. There is a reduction in velocity by increasing the micropolar fluid constant N_3(Fig. 9). Enhancement of micro inertial density causes N_3 to grow, so microrotation will decrease. Fig 10 shows that there are no changes in the microrotation profile with enhancement in Reynolds number Re. fig11 demonstrated that there was a reduction in the microrotation profile while parameter R increased. In fig 12, with accretion in the thermophoretic parameters, the temperature profile increased due to the enhancement of the thermodiffusion coefficient (DT). Fig 13 showed that there was a diminishing in temperature profile while the radiation parameter increased. The radiation parameter *Rd* defines the relative contribution of conduction heat transfer to thermal radiation transfer. Since the thermal radiation transfer grows faster than conduction heat transfer, the temperature profile decreases. According to fig 14, the concentration profile decreased with the increase of Brownian motion. It's obvious that with the increase in a random motion, concentration will decrease. Fig 15 illustrated that with the enhancement of the thermophoretic parameter, the concentration profile increased. With an increase in particles thermodiffusion concentration will increase. Fig 16 indicates that an increase in the Reynolds number causes a decrease in the concentration profile. Because of an increase in velocity, the concentration decreased. Fig 17 shows that with the enhancement of the Schmidt number, the concentration decreased due to the increase in the momentum diffusivity.

In fig 18, the upper side of the channel showed increases in the Nusselt number while Reynolds and radiation parameters were increased, but on the lower side, the Nusselt number decreased. On the upper side of the channel, certainly convective has higher amounts because there have to be two phases of fluids, but on the lower side, because of nanofluid properties, conductive have higher amounts. The same reason goes for fig 19, which indicates the effect of Reynolds and thermophoretic parameters on the Nusselt number.

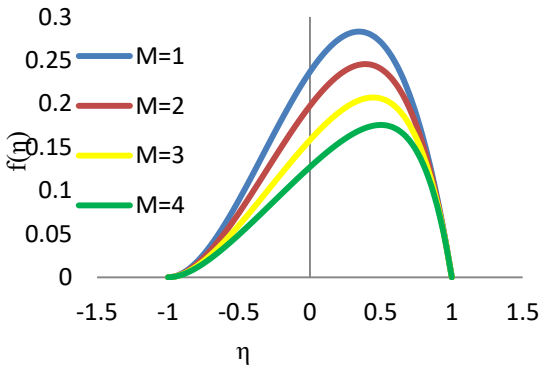

Figure 2: Velocity variations with the Hartmann number

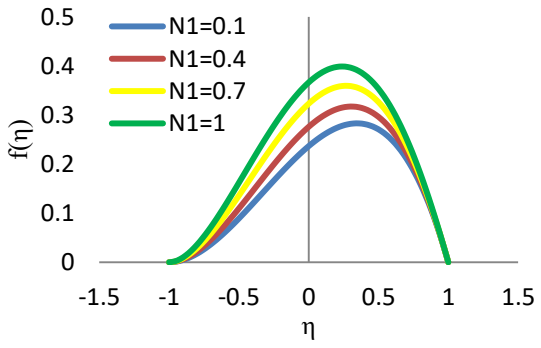

Figure 3: Velocity variations with N_1

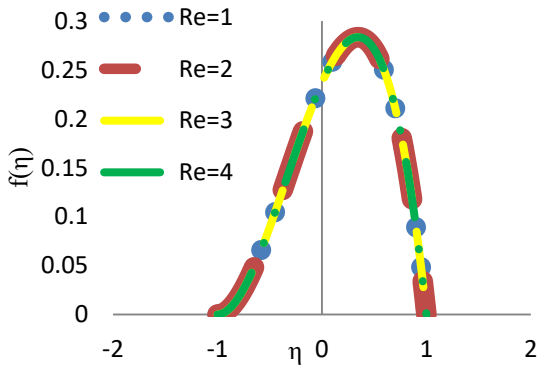

M=1,N2=0.2,N3=0.1,Nt=0.2,N1=0.1
Sc=0.2,Pr=6.2,Nb=0.2,Rd=0.2,R=0.1

Figure 4: Velocity variations with the Reynolds number

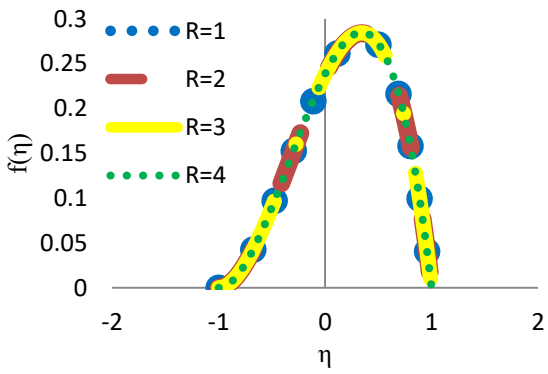

M=1,N2=0.2,N3=0.1,Nt=0.2,N1=0.1
Sc=0.2,Pr=6.2,Nb=0.2,Rd=0.2,Re=0.1

Figure 5: Velocity variations with the R parameter

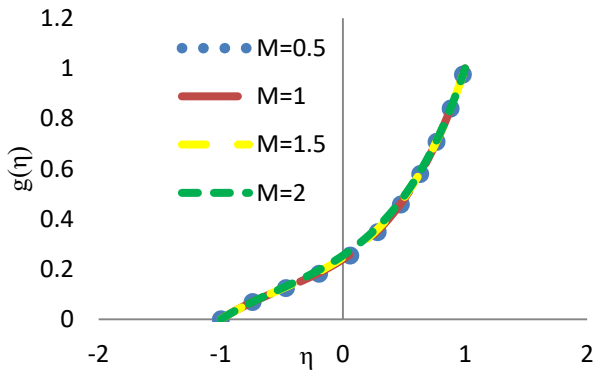

N2=0.2,N3=0.1,Nt=0.2,N1=0.1,Sc=0.2,Pr=6.2,
Nb=0.2,Rd=0.2,Re=0.1,R=0.1

Figure 6: Microrotation profile variations with Hartman number M

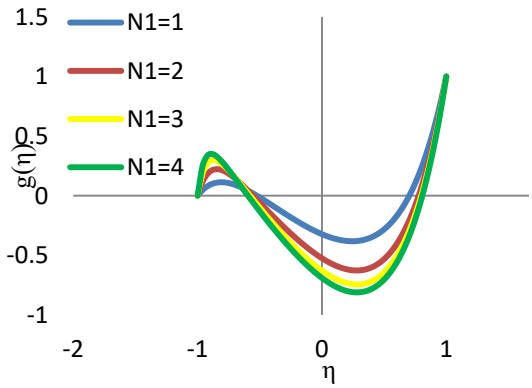

N2=0.2,N3=0.1,Nt=0.2,Sc=0.2,Pr=6.2,
Nb=0.2,Rd=0.2,Re=0.1,R=0.1,M=1

Figure 7: Microrotation profile variations with N_1

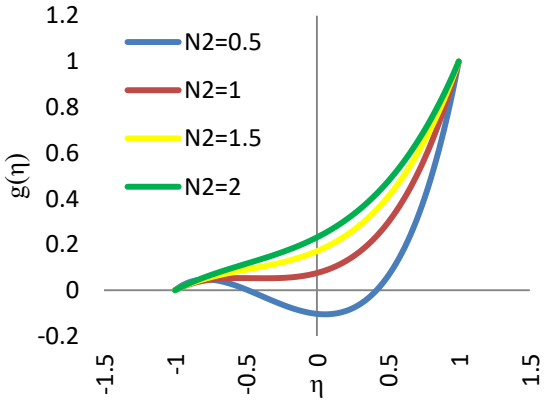

N1=0.1,N3=0.1,Nt=0.2,Sc=0.2,Pr=6.2,
Nb=0.2,Rd=0.2,Re=0.1,R=0.1,M=1

Figure 8: Microrotation profile variations with N_2

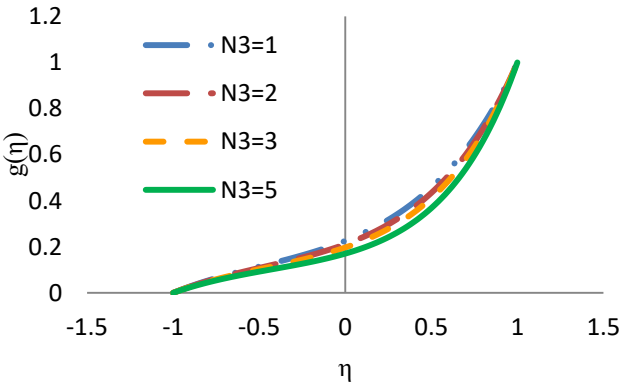

N1=0.1,N2=0.2,Nt=0.2,Sc=0.2,Pr=6.2,
Nb=0.2,Rd=0.2,Re=0.1,R=0.1,M=1

Figure 9: Microrotation profile variations with N_3

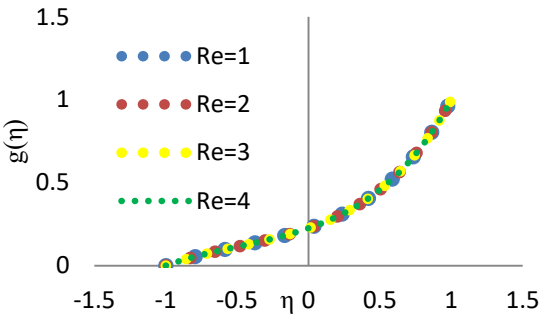

M=1,N1=0.1,N2=0.2,N3=0.1,Nt=0.2,Sc=0.2,
Pr=6.2,Nb=0.2,Rd=0.2,R=1

Figure 10: Microrotation profile variations with Re

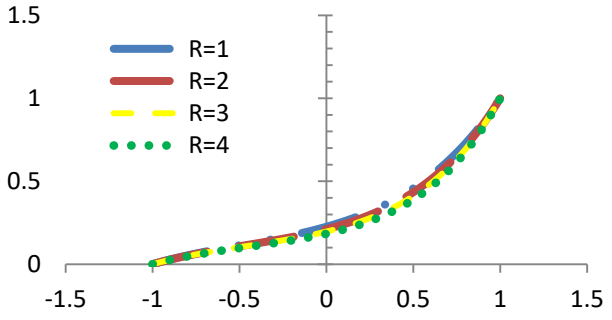

M=1,N1=0.1,N2=0.2,N3=0.1,Nt=0.2,Sc=0.2,Pr=6.2,Nb=0.2,Rd=0.2,
Re=1

Figure 11: Microrotation profile variations with R

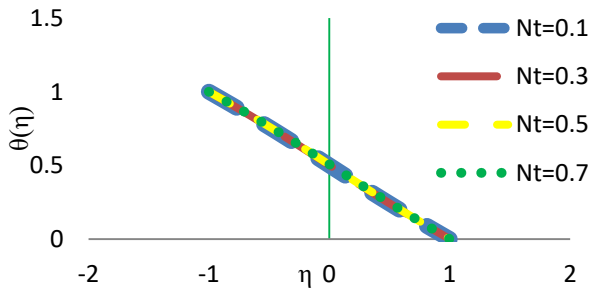

M=1,N1=0.1,N2=0.2,N3=0.1,Rd=0.2,
Sc=0.2,Pr=6.2,Nb=0.2,R=0.1,Re=0.1

Figure 12: Temperature profile variations for N_t

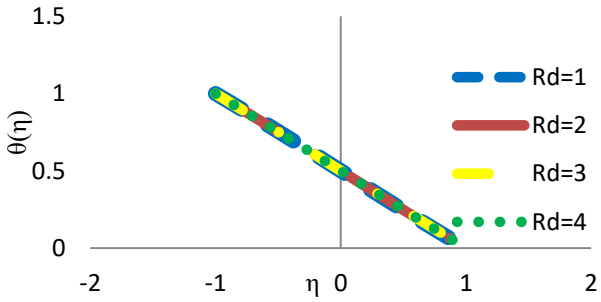

M=1,N1=0.1,N2=0.2,N3=0.1,Nt=0.2,
Sc=0.2,Pr=6.2,Nb=0.2,R=0.1,Re=0.1

Figure 13: Temperature profile variations Rd

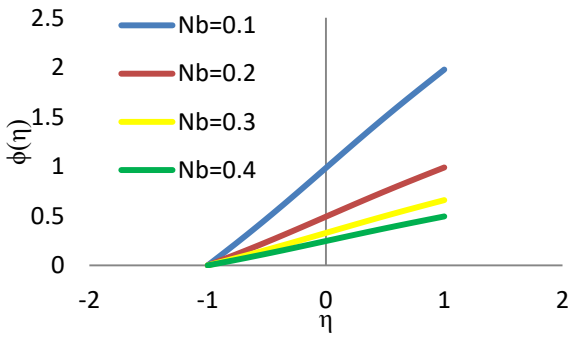

M=1,N1=0.1,N2=0.2,N3=0.1,Nt=0.2,
Sc=0.2,Pr=6.2,Rd=0.2,R=0.1,Re=0.1

Figure 14: Concentration profile variations with N_b

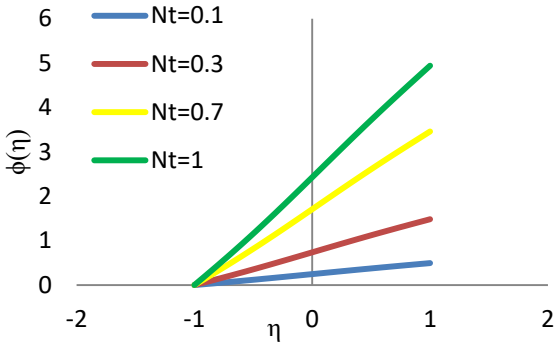

M=1,N1=0.1,N2=0.2,N3=0.1,Sc=0.2,
Pr=6.2,Nb=0.2,Rd=0.2,R=0.1,Re=0.1

Figure15: Concentration profile variations with N_t

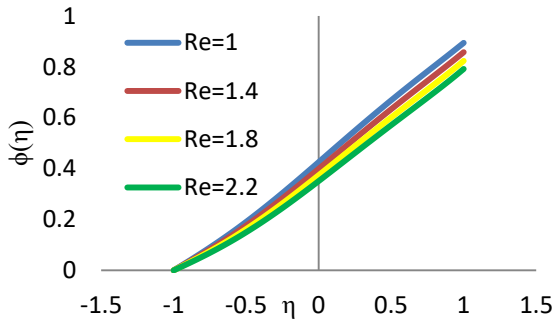

M=1,N1=0.1,N2=0.2,N3=0.1,Nt=0.2,
Sc=0.2,Pr=6.2,Nb=0.2,Rd=0.2,R=0.2

Figure 16: Concentration profile variations with Re

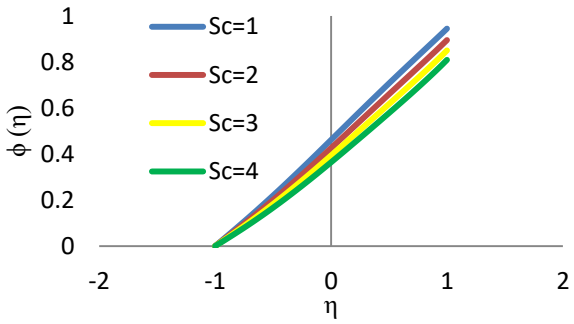

M=1,N1=0.1,N2=0.2,N3=0.1,Nt=0.2,
Pr=6.2,Nb=0.2,Rd=0.2,R=0.1,Re=0.1

Figure 17: Concentration profile variations with Sc

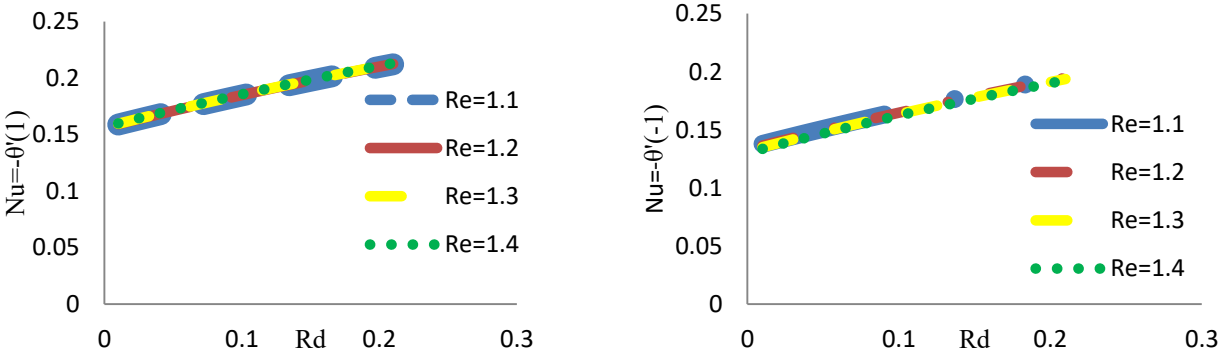

M=1,N1=0.1,N2=0.2,N3=0.1,Nt=0.1,Sc=0.1,Pr=6.2,Nb=0.1,R=1.1

Figure 18: Effect of Reynolds number and radiation parameter on Nusselt number

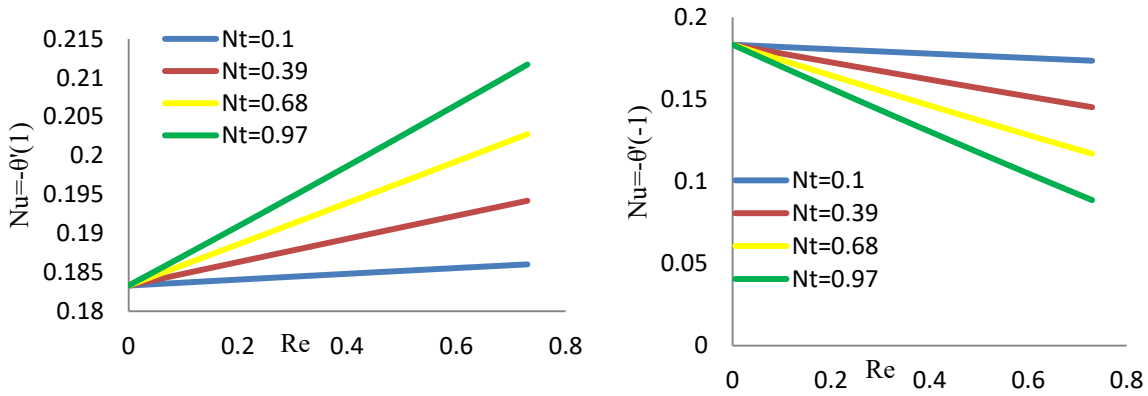

N1=0.1,N3=0.1,Nb=0.1,Sc=0.1,Rd=0.1,N2=0.2,Pr=6.2,M=1,R=1.1

Figure 19: Effect of Reynolds number and thermophoresis parameter on Nusselt number

4. Verification with AGM Method

Due to the fact that there is a huge amount of difference in some results, especially in temperature and concentration profile with previous works, the AGM method is used to verify the results.

As in previous work mentioned before [6], [7] AGM method suggests that answers to the ODEs can be shown as polynomial shapes. In this article, the assumption which gave answers suggests that:

$$f(x) = \sum_{i=0}^{7} a_i\, x^i \;\; , g(x) = \sum_{i=0}^{7} b_i\, x^i \;\; , \theta(x) = \sum_{i=0}^{5} c_i\, x^i \;\; , \phi(x) = \sum_{i=0}^{5} d_i\, x^i \qquad (4)$$

Now, all it takes is to find the coefficients, a_i , b_i , c_i and d_i. At first, by putting boundary conditions (2) into series (4) ten equations will obtain as follow:

$$a_0 - a_1 + a_2 - a_3 + a_4 - a_5 + a_6 - a_7 = 0 \quad (5)$$

$$a_1 - 2\,a_2 + 3\,a_3 - 4\,a_4 + 5\,a_5 - 6\,a_6 + 7\,a_7 = 0 \quad (6)$$

$$a_0 + a_1 + a_2 + a_3 + a_4 + a_5 + a_6 + a_7 = 0 \quad (7)$$

$$a_1 + 2\,a_2 + 3\,a_3 + 4\,a_4 + 5\,a_5 + 6\,a_6 + 7\,a_7 = -1 \quad (8)$$

$$b_0 - b_1 + b_2 - b_3 + b_4 - b_5 + b_6 - b_7 = 0 \quad (9)$$

$$b_0 + b_1 + b_2 + b_3 + b_4 + b_5 + b_6 + b_7 = 1 \quad (10)$$

$$c_0 - c_1 + c_2 - c_3 + c_4 - c_5 = 1 \quad (11)$$

$$c_0 + c_1 + c_2 + c_3 + c_4 + c_5 = 0 \quad (12)$$

$$d_0 - d_1 + d_2 - d_3 + d_4 - d_5 = 0 \quad (13)$$

$$0.2\,d_1 + 0.4\,d_2 + 0.6\,d_3 + 0.8\,d_4 + 1.0\,d_5 + 0.1\,c_1 + 0.2\,c_2 + 0.3\,c_3 + 0.4\,c_4 + 0.5\,c_5 = 0 \quad (14)$$

Other 18th equation which is needed for solving the system of polynomials will be achieved by applying series (4) to equations (1) and by use of boundary conditions (2) and by derivation from them all required equations will be produced.

In fig 20 there is a comparison between the finite element and the AGM method to validate the current result.

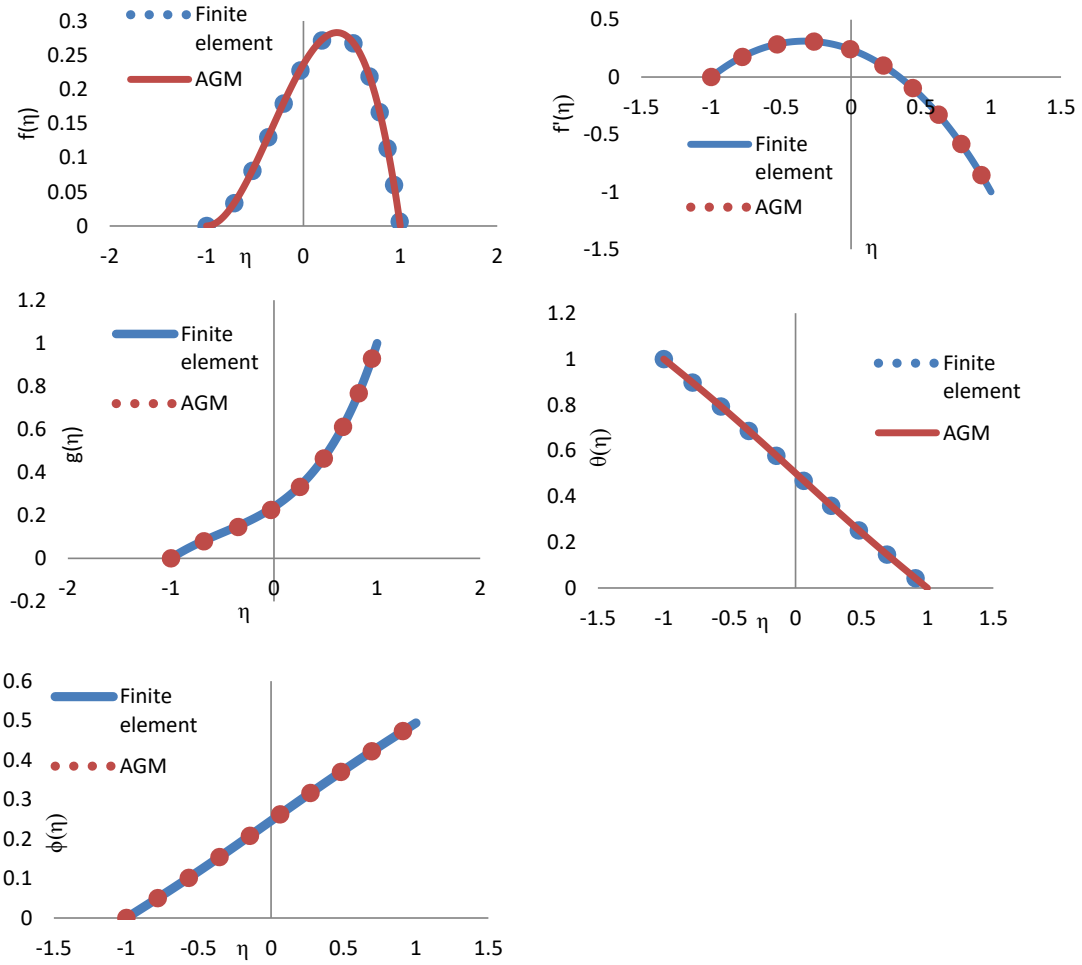

Figure 20: comparer between AGM and finite element method for M=1,N1=0.1,N2=0.2,N3=0.1,Sc=0.2,Pr=6.2,Nb=0.2,R=0.1,Rd =0.2,Nt=0.1,Re=0.1

5. Conclusion

Radiative micropolar nanofluid passed through a porous channel has been studied with finite element and AGM methods. The effect of the coupling parameter $N_1$and the parameter R was to increase the variation of velocity while Hartman number M decreased it. Hartman number M and spin gradient viscosity N_2 enhanced the microrotation profile although the coupling parameter N_1, micropolar fluid constant N_3 and parameter R reduced the microrotation profile. Thermophoretic parameter N_t raised the temperature profile but the radiation parameter R_d dropped it. Thermophoretic parameter N_t magnified the concentration profile, unlike Brownian motion N_b and Schmidt number S_c which declined the concentration profile. Reynolds number Re had no change in the variation of velocity and microrotation profile, while it decreased the concentration profile.

Nomenclature

a,b,c,d	*AGM coefficient*	S_c	*Schmidt number*
B	*Magnetic field*	T	*Fluid temperature*
C	*Concentration of the fluid*	T_1	*Temperature at the lower plate of the channel*
C_1	*Concentration at the lower plate of the channel*	T_2	*Temperature at the upper plate of the channel*
C_2	*Concentration at the upper plate of the channel*		
D_B	*Brownian diffusion coefficient*	$\hat{\kappa}$	*Vertex viscosity*
D_T	*Thermophoretic diffusion coefficient*	μ	*Dynamic viscosity*
j	*Microinertiai density*	υ	*Kinamatic cofficent*
k	*Thermal conductivity*	ρ	*Density*
M	*Hartman number*	f	*Dimensionless stream function*
N_1	*Coupling parameter*	g	*Dimensionless form of the microrotation profile*
N_2	*Spin gradient viscosity parameter*	θ	*Dimensionless temperature profile*
N_3	*Micropolar fluid constant*	ϕ	*Dimensionless concentration profile*
N_b	*Brownian motion*	P_r	*Prandtl number*
N_t	*Thermophoretic parameter.*	η	*Dimsensionless similarity variable*
N_u	*Nusselt number*	σ	*Electric conductivity*
Re	*Reynolds number*	α	*Thermal diffusivity*
R_d	*Redation parameter*		

References

1. Kausar, M. S., Hussanan, A., Waqas, M., & Mamat, M. (2022). Boundary layer flow of micropolar nanofluid towards a permeable stretching sheet in the presence of porous medium with thermal radiation and viscous dissipation. Chinese Journal of Physics, 78, 435-452.
2. Mathur, P., & Mishra, S. (2022). Adomian Decomposition Method for the Radiative Micropolar Nanofluid Past a Porous Channel: An Analytical Approach.
3. Sheikholeslami, M., Ashorynejad, H. R., Ganji, D. D., & Rashidi, M. M. (2014). Heat and mass transfer of a micropolar fluid in a porous channel. Commun Numer Anal, 2014(2).
4. Mohyud-Din, S. T., Jan, S. U., Khan, U., & Ahmed, N. (2018). MHD flow of radiative micropolar nanofluid in a porous channel: optimal and numerical solutions. Neural Computing and Applications, 29, 793-801.
5. Takhar, H. S., Bhargava, R., Agrawal, R. S., & Balaji, A. V. S. (2000). Finite element solution of micropolar fluid flow and heat transfer between two porous discs. International journal of engineering science, 38(17), 1907-1922.
6. Jalili, P., Narimisa, H., Jalili, B., Shateri, A., & Ganji, D. D. (2023). A novel analytical approach to micro-polar nanofluid thermal analysis in the presence of thermophoresis,

Brownian motion and Hall currents. Soft Computing, 27(2), 677-689.
7. Jalili, P., Narimisa, H., Jalili, B., & Ganji, D. D. (2023). Micro-polar nanofluid in the presence of thermophoresis, hall currents, and Brownian motion in a rotating system. Modern Physics Letters B.
8. Shah, Z., Islam, S., Gul, T., Bonyah, E., & Khan, M. A. (2018). The electrical MHD and hall current impact on micropolar nanofluid flow between rotating parallel plates. Results in physics, 9, 1201-1214.